# H/D-Isotope fractionation due to aqueous phase diffusion – deuterated hydrocarbons revisited

Frank-Dieter Kopinke*, Anett Georgi

Helmholtz Centre for Environmental Research – UFZ, Department of Environmental Engineering, D-04318 Leipzig, Germany

*Corresponding author. Fax: +49 341235451234.

*E-mail address:* frank-dieter.kopinke@ufz.de

GRAPHICAL ABSTRACT

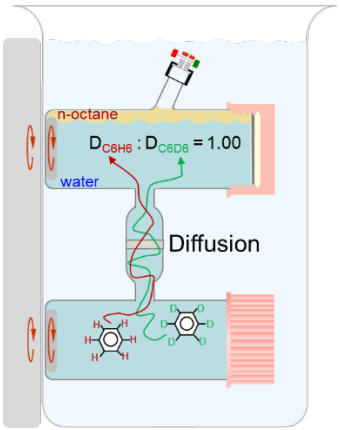


## ABSTRACT

Diffusive isotope fractionation of non- and perdeuterated benzenes and toluenes in aqueous solution was investigated. The experimental method was based on a Stokes diaphragm cell. The isotope composition of diffusate and retentate was found to be identical within a range of uncertainty of ± 5‰ for benzene and ± 10‰ for toluene. These data are consistent with a previous fractionation study using phase-transition kinetics as the potentially fractionating step. The present study contributes to strengthening the data base for diffusive isotope fractionation of organic compounds in aqueous solution. According to the presented data, diffusion of naturally occurring,

monodeuterated organic compounds does not significantly affect their hydrogen isotope pattern.

*Keywords:* isotopic fractionation, aqueous phase diffusion, deuterated organic compounds, diaphragm cell.

*Highlights:*

- Aqueous-phase diffusion does not significantly fractionate perdeuterated benzenes.
- Diffusive fractionation does not significantly affect the hydrogen isotope pattern of naturally occurring organic compounds.
- Different experimental diffusion setups yield diverging fractionation data.

## 1. Introduction

Stable isotope methods have become firmly established as a powerful tool for describing and understanding the fate of chemicals in the environment (Hunkeler et al., 2009; Elsner, 2010; Elsner et al. 2012; Thullner et al., 2012; Wanner and Hunkeler, 2019 and refs. cited therein). They are based on shifts in isotope composition of a target compound due to chemical reactions or physical processes. Usually, physical processes such as adsorption, volatilization or diffusion are less fractionating than chemical reactions where chemical bonds are broken and formed. Nevertheless, even physical processes can cause significant isotope fractionation due to accumulation of small elemental effects, e.g. by a large number of successive adsorption-desorption steps along a flow path (Kopinke et al., 2005). It is not *a priori* clear whether diffusion-induced isotope fractionation may play a significant role for the interpretation of solutes' isotope patterns in an aquifer and even more importantly in aquitards where diffusive transport may dominate over convective transport.

Recently, Wanner and Hunkeler (2019) have reviewed the “Isotope fractionation due to aqueous phase diffusion…” in this journal. They placed a special focus on the comparison between experimental data and the ability of various diffusion models to explain and predict fractionation effects. The review covers a number of ions, noble gases and organic compounds with hydrogen, carbon and chlorine as isotope targets. Fractionation experiments can be conducted either with naturally occurring isotopologues or with isotopically labelled compounds. With respect to deuterated compounds, Wanner and Hunkeler (2019) state that “the obtained results (in literature) were not consistent” and that there are “doubts on whether deuterated compounds are representative for studies of isotope fractionation during aqueous phase diffusion at natural abundance”. Due to the low natural abundance of deuterium (0.015 at-%), only monodeuterated isotopologues do appear in nature. It is a matter for discussion, whether their fractionation behaviour can or cannot be derived from that of highly deuterated isotopologues.

Diffusive fractionation data on deuterated compounds are scarce in the literature and, to the best of our knowledge, they have only been measured with perdeuterated isotopologues. Fractionation effects are usually presented as a ratio of diffusion coefficients $\alpha_{diff} = D_{heavy}/D_{light}$ (diffusion isotope effect) or as a kinetic fractionation factor $\alpha_{kin} = k_{heavy}/k_{light}$, wherein $k_i$ (in m $s^{-1}$) are mass-transfer coefficients and $D_i$ (in $m^2$ $s^{-1}$) are diffusion coefficients of the heavy and the light isotopologues. $\alpha$-values are mostly very close to 1. Therefore, it may be convenient to convert them into $\varepsilon$-values according to $\varepsilon = (\alpha - 1) \bullet 1000$ in ‰. The two fractionation parameters $\alpha_{diff}$ and $\alpha_{kin}$ can be correlated according to $k_1/k_2 = (D_1/D_2)^n$, because mass-transfer processes frequently include diffusion as the rate-limiting step. Depending on the mass-transfer model applied, the exponent $n$ can have values between 1 (film model) and ½ (surface

renewal model) (Schwarzenbach et al., 2003). For rigid and smooth interfaces, the Deacon model (Deacon, 1973) with $n$ = 2/3 is frequently applied.

Table 1 collects the available data base for diffusive fractionation of deuterated compounds, together with some recent data on fractionation of noble gas isotopes.

**Table 1:** Isotope effects for diffusion of noble gases and deuterated hydrocarbons in water from literature studies (T = (20 ± 5)°C)

| Isotopes and isotopologues ($R_{van\ der\ Waals}$ in pm) [2)] | $D_{heavy}/D_{light}$ or $k_{heavy}/k_{light}$ [1)] | Method applied | Literature source |
|---|---|---|---|
| $^{4}He$ / $^{3}He$ (140) | **0.87** ± 0.03 | modified Barrer method with water gel diaphragm | Jähne et al., 1987 |
| $^{22}Ne$ / $^{20}Ne$ (154) | 0.990 ± 0.003 | gel diffusion cell between 2 purged gas chambers | Tyroller et al., 2014 |
| | 0.9931 ± 0.0004[1)] | relative mass-transfer rates across a water-gas interface | Tempest and Emerson, 2013 |
| $^{40}Ar$ / $^{36}Ar$ (188) | **0.948** ± 0.004 | gel diffusion cell between 2 purged gas chambers | Tyroller et al., 2014 |
| | 0.9961 ± 0.0001[1)] | relative mass-transfer rates across a water-gas interface | Tempest and Emerson, 2013 |
| | 0.9963 ± 0.0003[1)] | relative mass-transfer rates across a water-gas interface | Seltzer et al., 2019 |
| $^{86}Kr$ / $^{84}Kr$ (202) | 0.9965 ± 0.0026 | 1-D gel dissection tubes | Tyroller et al., 2018 |
| $^{84}Kr$ / $^{82}Kr$ (202) | 0.9995 ± 0.0012 | relative mass-transfer rates across a water-gas interface | Seltzer et al., 2019 |

| | | | |
|---|---|---|---|
| $^{86}Kr$ / $^{82}Kr$ (202) | 0.9986 ± 0.0003[1)] | relative mass-transfer rates across a water-gas interface | Seltzer et al., 2019 |
| $^{136}Xe$ / $^{132}Xe$ (216) | 0.9993 ± 0.0010 | 1-D gel dissection tubes | Tyroller et al., 2018 |
| $^{136}Xe$ / $^{129}Xe$ (216) | 0.9990 ± 0.0004[1)] | relative mass-transfer rates across a water-gas interface | Seltzer et al., 2019 |
| $C_6D_6$ / $C_6H_6$ (255) | 1.00 ± 0.01[1)] | relative mass-transfer rates across dynamic aqueous boundary layers | Kopinke et al., 2018 |
| | **1.019** ± 0.002 | 1-D gel dissection tubes | Rolle and Jin, 2017 |
| $C_7D_8$ / $C_7H_8$ (271) | 1.00 ± 0.01[1)] | relative mass-transfer rates across dynamic aqueous boundary layers | Kopinke et al., 2018 |
| | **0.962** ± 0.002 | 1-D gel dissection tubes and | Jin et al., 2014 |
| | **0.962** ± 0.002 | modelling of 2-D flow through system | Rolle and Jin, 2017 |
| $C_6D_5$-$C_2D_5$ / $C_6H_5$-$C_2H_5$ (335) | **0.961** ± 0.003 | 1-D gel dissection tubes | Jin et al., 2014 |
| | **0.95** [3)] | estimated by modelling of transverse dispersion in a porous flow-through cell | Rolle et al., 2010 |
| c-$C_6D_{12}$ / c-$C_6H_{12}$ (290) | 1.00 ± 0.01[1)] | relative mass-transfer rates across dynamic aqueous boundary layers | Kopinke et al., 2018 |
| $(CD_3)_2CD$-OH / $(CH_3)_2CH$-OH (257) | 0.993 [3)] | Taylor dispersion method | LaBolle et al., 2008 |

| | | | |
|---|---|---|---|
| $(CD_3)_3C$-OH / $(CH_3)_3C$-OH (276) | 0.997 [3)] | Taylor dispersion method | LaBolle et al., 2008 |

[1)] Ratio of mass-transfer coefficients; [2)] van der Waals radii for noble gases from Wikipedia, for benzene and toluene from Gabler et al. (1996), for other compounds calculated with JCHEM for Microsoft Excel; [3)] error ranges not available.

Noble gases were included in Table 1, because there are some similarities between them and the investigated hydrocarbons (range of atomic masses, atom or molecule size, non-charged, hydrophobicity). The most recent review of Wanner and Hunkeler (2019) had not yet considered the recent studies of Kopinke et al. (2018), with fractionation data for benzene, toluene and cyclohexane, and of Seltzer et al. (2019) for Ar, Kr and Xe isotopes, which are integrated in Table 1. It is obvious from Table 1 that the available data on diffusive isotope effects are not consistent, neither for deuterated hydrocarbons nor for argon as diffusant. Most of the fractionation effects for isotopes and isotopologues are rather small, i.e. $|\varepsilon| \leq 10‰$ (compare also the data collection of Wanner and Hunkeler (2019), Table 2 there). However, there are some exceptions, which are highlighted in Table 1: Jin et al. (2014) found strong fractionation effects for toluene and ethylbenzene ($D_{C7D8}/D_{C7H8} = 0.962 \pm 0.002$ and $D_{C8D10}/D_{C8H10} = 0.961 \pm 0.003$). Rolle and Jin (2017) confirmed the value for toluene, but found a significant inverse fractionation effect for benzene ($D_{C6D6}/D_{C6H6} = 1.019 \pm 0.002$). The inversion of the diffusive isotope effect for the two very similar solutes, benzene and toluene, is hard to interpret. These findings are clearly inconsistent with results from Kopinke et al. (2018) who found that “for all investigated solutes (benzene, toluene and cyclohexane) there was no significant observable fractionation effect between

nondeuterated and perdeuterated isotopologues, resulting in $D_{heavy}$ : $D_{light}$ = 1.00 ± 0.01". The applied method was based on liquid-liquid and liquid-gas partitioning experiments under kinetic control. Derivation of relative diffusion coefficients from mass-transfer kinetics assumes a molecular diffusion step to be rate-controlling in the phase-transfer kinetics. Although this is in accordance with the established doctrine (Schwarzenbach et al., 2003; Cussler, 2009), the obvious discrepancy between the results of dynamic and static diffusion systems motivated us to perform further investigations. It is worth mentioning that the large fractionation effects were observed with the same method: diffusion along static 1-D gel dissection tubes; however, they were also qualitatively confirmed by 2-D flow-through experiments.

It is the aim of the present study to verify isotope fractionation in diffusion of BTX with an additional independent experimental technique based upon a diaphragm cell, which is a well established method (Cussler, 2009; Wanner and Hunkeler, 2015). Four diffusants were included in this study: benzene-$D_0$, benzene-$D_6$, toluene-$D_0$ and toluene-$D_8$.

## 2. Materials and methods

### *2.1. Chemicals*

All non-labelled chemicals were obtained from Merck (Germany) in the highest available purity. The deuterated compounds were obtained from Roth (Germany, $C_6D_6$) and Chemotrade (Germany, $C_7D_8$).

### *2.2. The diffusion cell*

We used a diaphragm cell with a horizontal glass frit (porosity P16 corresponding to G4: 10-16 µm pore width, cross section area about 5 $cm^2$, thickness about 3 mm) as diffusion layer, as depicted in Figure 1.

→ Please insert **Figure 1** here: Experimental set-up with diaphragm diffusion cell. Gaseous or liquid samples can be taken from the Mininert™ valve.

The upper compartment was equipped with a glass branch and a Mininert™ valve for sampling. The two compartments have equal volumes of about 100 mL. The source compartment was completely filled with deionized water. The destination compartment contained 90 to 100 mL of water. The remainder was 5 mL of gas headspace or contained additional 10 mL of n-octane as *in-situ* extractant. Both compartments were first purged with carbon dioxide, then filled with deionized water and purged with a helium flow for several hours under stirring prior to spiking, in order to fill the frit with water and to avoid any degassing during the diffusion experiment. Microbiological activity was inhibited by adding 100 mg $L^{-1}$ sodium azide. The four diffusants were spiked from a common ethanolic stock solution (50 µL of 4 × 40 g $L^{-1}$) in the source compartment (initial concentration $C_{0,i}$ = 20 mg $L^{-1}$ of each isotopologue). The diffusion experiment was started ($t$ = 0) when the two magnetic stirrers (glass wall coated) were started. The intensity of stirring was adjusted for intensive mixing of the two water phases, while avoiding dispersion of the n-octane phase (if present) into the upper water phase.

Two types of diffusion experiments were conducted: (i) with headspace sampling and (ii) with *in-situ* liquid-liquid extraction of the diffusants. In the extraction series, 10 mL of water were replaced by 10 mL of n-octane in the upper compartment prior to starting the experiment.

Special emphasis was placed on the long-term leak-tightness and inertness of the two compartments. All possible sorptive sinks were avoided (except for the n-octane phase when intentionally applied). In order to achieve this, the screw-openings of the two compartments were covered with PTFE-lined silicone septa which were additionally made inert by means of thin aluminium foils. The screw threads were sealed with thin PTFE bands.

The sampling of gas or n-octane samples from the destination compartment was performed with micro-syringes through a Mininert™ valve which contained only PTFE parts in direct contact with the analytes. The entire cell, including sampling device, was placed in a water-filled basin underneath its water table in order to avoid gas leaks and temperature gradients. The experiments with n-octane as extractant were *a priori* insensitive for loss of analytes because the organic phase acts as a sink for them.

Both cell compartments were independently stirred by glass-coated stirrer bars, ensuring a fast and complete mixing of the two bulk phases.

### *2.3. Sampling and isotope analysis*

The diffusion process between the two water-filled compartments was monitored by sampling the headspace phase (25 µL gas-tight microsyringe) or the octane phase (100 µL). The bottom compartment could not be sampled and analysed during the diffusion experiments. Instead, two water reference samples were prepared in the same way from the same stock solution as the source compartment, sampled and analysed under identical conditions.

At the end of each diffusion experiment (usually after 10 to 60 d), the two compartments were opened. The octane phase from the upper compartment (*in-situ* extraction experiments) was withdrawn for analysis. The source compartment and, where

appropriate, the destination compartment were extracted with 10 mL of n-octane. These extracts were analysed together with the reference extracts.

The gaseous headspace samples and the octane extracts were analysed by means of gas chromatography with quadrupole mass spectrometer detection (GC-MS QP2010 ultra, Shimadzu) in the selected ion monitoring (SIM) mode. The solute's isotopologues were quantified by precise peak area integration of their molecule and most intense fragment ion signals (m/z = 78 and 84 amu for $C_6H_6$ and $C_6D_6$ as well as m/z = 92 + 91 and 100 + 98 amu for $C_7H_8$ and $C_7D_8$, respectively). The analyte's peak areas were kept in an optimal range by sample dilution and variation of the GC conditions (injector split ratio) in order to avoid any peak discrimination. It was verified that the measured ratio of peak areas (e.g. $A_{78}/A_{84}$) was constant (deviation $\leq \pm 0.5\%$) over a range of three orders of magnitude in the analyte's sample concentration for a given isotopologue mixture. The reproducibility of measured peak area ratios for a given sample was in the range of $\pm$ 1‰ (one estimate of standard deviation of single values) for gas samples and slightly worse for liquid samples ($\pm$ 2‰).

The GC conditions were as follows: 30 m DB1 column, 0.32 mm inner diameter, 5 µm film thickness, $T_{\text{injector}}$ = 250°C, $T_{\text{oven}}$ = 70°C isotherm for 25 µL gaseous sample injection, $T_{\text{oven}}$ = 35°C (1 min), 20 K $\text{min}^{-1}$ up to 80°C (10 min) for 0.5 µL liquid sample injection, $p_{\text{He}}$ = 0.25 MPa, split ratio 10:1. MS conditions: $T_{\text{interface}}$ = $T_{\text{ion source}}$ = 250°C, EI with 70 eV, SIM mode with m/z = 77, 78, 83, 84, 91, 92, 98, 100 amu, gain 0.93 kV, scan time 0.3 s.

## 3. Results and discussion

### *3.1. Analytics*

The main data which characterize diffusive isotope fractionation are relative concentrations or relative GC peak areas, comparing isotope composition of the diffusants in the two aqueous compartments, the source compartment and the destination compartment. In order to minimize systematic biases of these values we arranged similar sampling and analysis conditions for the associated samples: headspace (gas) samples were compared with headspace samples only and liquid samples (n-octane extracts) were compared with liquid samples only. In addition, reference samples were adjusted in their analyte concentrations (from the same stock solution) such that they were in the same concentration range as the diffusion samples. For quantitation of isotope data, only pairs from GC-MS measurements performed on the same day were used. In this way, small shifts in GC-MS stability could be minimized.

→ Please insert **Figure 2** here: Example of GC-MS isotope analyses of benzenes: ratios of peak areas for ion traces m/z = 78 amu ($A_{78}$) and m/z = 84 amu ($A_{84}$) for samples (n-octane extracts) of a typical diffusion experiment along the analysis numbers within a series of successive analyses. The lines are guides for the eyes only.

Figure 2 shows a typical set of benzene isotope analyses where n-octane samples, collected at various times out of a 17 d diffusion experiment, were analysed on the same day together with a reference sample. The first 10 chromatograms of the series revealed an increasing ratio of peak areas for $C_6H_6$ (m/z = 78) and $C_6D_6$ (m/z = 84).

They served for conditioning of the ion source of the mass spectrometer. Only when the peak ratios approached stable values were the sample data collected for reliable isotope analyses. At the end of a 50-injection series, the same reference sample was analysed again in order to confirm the stability of the mass spectrometer.

Although the precision of gas analyses ($\sigma(A_{78}/A_{84}) = \pm 1‰$) was better than for liquid octane samples ($\sigma(A_{78}/A_{84}) = \pm 2‰$), the liquid-liquid extraction was finally applied due to a better long-term stability of the diffusion cell (see discussion below). The precision of the analytical data was further improved by performing 5 to 10 repetition analyses for the final extract samples.

### *3.2. Mathematical treatment of the diffusion cell*

The mass transfer between the two compartments of a diaphragm cell can be described by first-order kinetics based upon Fick's first law, assuming a linear concentration gradient across the diaphragm length.

$$dN_i / dt = D_i \bullet A \bullet H / L \bullet (C_{source,i} - C_{destin,i}) \quad (1)$$

with $dN_i/dt$ as molar flux (in mol $s^{-1}$), $D_i$ as diffusion coefficient (in $cm^2$ $s^{-1}$) of the diffusant *i* in water, *A* as the cross area of the diaphragm (in $cm^2$), *H* (without units) as a fitting parameter which includes the fraction of the diaphragm's area that is available for diffusion, *L* as the thickness of the diaphragm (in cm) and $C_{source,i} - C_{destin,i}$ as the diffusant's concentration difference (in mol $L^{-1}$) between the two cell compartments. This rate equation can be integrated, simplified (under the condition $C_{destin} << C_{source}$) and rearranged (see SI part) leading finally to eq. 2. It delivers the ratio of two diffusion coefficients, e.g. $D_{heavy}/D_{light}$ for the heavy and the light isotopologues of a compound, from measurement of diffusant's relative concentrations.

$$\frac{D_{heavy}}{D_{light}} = \frac{\ln[(C_{source,heavy} - C_{destin,heavy})_t / C_{source,heavy,0}]}{\ln[(C_{source,light} - C_{destin,light})_t / C_{source,light,0}]} \quad (2)$$

It is worthy of note that the two applied operation regimes of the diffusion cell have consequences for data handling. The diffusion between the two water compartments is a reversible process, finally leading to equal concentrations (more precisely to equal activities) in them. With n-octane as sink above the destination compartment, the diffusive flux becomes largely irreversible. It follows that $C_{source,i,t\to\infty} = C_{destin,i,\ t\to\infty} \approx 0$. As discussed in chapter 3.4, we applied mainly the irreversible diffusion regime. Therefore, the corresponding formulas will only be derived for this case.

The most significant and reliable quantity for isotope fractionation is the ratio of concentrations of component pairs in the upper and the lower compartment of the diaphragm cell after termination of the diffusion experiment. We denominate this as $R$.

$$R = \left(\frac{C_{light}}{C_{heavy}}\right)_{destin} / \left(\frac{C_{light}}{C_{heavy}}\right)_{source} \quad (3)$$

$R$ can be described as a function of two simultaneous diffusive mass-transfer processes with rate coefficients $k_{light}$ and $k_{heavy}$ for the diffusion of the light and the heavy isotopologue of a diffusant, respectively.

$$R = \frac{1 - e^{k_{light} \times t}}{1 - e^{k_{heavy} \times t}} \quad (4)$$

The rate coefficients are directly proportional to the corresponding diffusion coefficients such that eq. 5 follows:

$$\frac{k_{heavy}}{k_{light}} = \alpha_{kin} = \frac{D_{heavy}}{D_{light}} = \alpha_{diff} = \frac{1000 + \varepsilon_{diff}}{1000} \quad (5)$$

267 $\alpha_{diff}$ and $\varepsilon_{diff}$ (in ‰) are commonly named as fractionation factor and enrichment factor,
268 respectively (Coplen, 2011). It is important to note that the exponent *n* for the
269 transformation $\alpha_{kin} = \alpha_{diff}^{n}$ is one, independent of assumptions about the mass-transfer
270 regime, because the mass transfer is purely diffusive in the diaphragm cell. Eqs. 4 and
271 5 can be rearranged such that $\alpha_{diff}$ can be directly calculated from measured values
272 $R(t)$ and $t$ or, alternatively, extents of diffusion $X_{diff} = 1 - \exp(-k \bullet t)$, where $X_{diff}$ is specified
273 as extent of diffusion of the light isotopologue ($X_{light}$) in eq. 6.

274 $$\alpha_{diff} = \frac{\ln [1 + X_{light}/(R \times (1 - X_{light})]}{\ln [1/(1 - X_{light})]} \quad (6)$$

275 A more detailed derivation of the formulas is described in the SI part. Qualitatively, one
276 can already derive from the observation that the isotope composition of the diffusate
277 (= destination compartment) and the retentate (= source compartment) are equal
278 (within the error range), i.e. $R \approx 1.00$ at any diffusion time, that the isotope fractionation
279 factor $\alpha_{diff}$ is close to 1.00 and the enrichment factor $\varepsilon_{diff}$ is close to zero. This is our
280 general finding for deuterated benzenes and toluenes in aqueous diffusion, as will be
281 outlined in the next chapters.
282
283 *3.3. Expected results for toluene fractionation*
284 Rolle and Jin (2017) as well as Jin et al. (2014) measured strong isotope fractionation
285 between toluene-$D_0$ and toluene-$D_8$ during diffusion in 1-D aqueous gel dissection
286 tubes. The consequences of such a fractionation with $\alpha_{diff} = 0.962 \pm 0.002$ for isotope
287 patterns in a diaphragm cell, as was applied in the present study, are illustrated in
288 Figure 3. The light toluene would diffuse about 4% faster than the heavy isotopologue.
289

→ Please, insert **Figure 3** here: Isotope fractionation in a diffusion process with a sink in the destination compartment according to the setup in Figure 1. Curves are calculated with $D_{heavy}/D_{light}$ = 0.962. The concentration ratios at the Y-axis are normalized to the initial composition in the source compartment at $t$ = 0, except for the dashed (red) curve, which represents the isotopologue ratios in the two compartments.

With progress of diffusion (X-axis), the toluene in the source compartment and in the destination compartment becomes heavier. The isotope ratio $R$ (red, dashed curve) increases steadily from $R_{t\rightarrow 0} = \alpha_{diff}$ towards higher values. The fractionation measurement becomes more sensitive as the diffusion progresses. However, the gain in sensitivity has to be paid for with long times of operation, because the progress in diffusion is exponentially correlated with time. Moderate diffusion times (≤ 2 months) are more feasible. It is clear from Figure 2 that isotope measurements with a precision of better than ± 1%, as applied in the present study, would be able to detect such large fractionation effects in a diaphragm cell. However, we did not observe such fractionation effects.

### *3.4. Operation regimes of the diffusion cell*

One of the most experienced experts in diffusion measurements, E. L. Cussler, characterized the diaphragm cell method (Stokes cell) with the following statement: “The final point about this method is its occasional unreliability...” (Cussler, 2009, p. 148). Indeed, we were also faced from time to time with inconsistent diffusion data without apparent reasons. Therefore, we introduced as a criterion of reliability of our experiments that the relative diffusion rates of benzene and toluene had to be close to the expected value of $D_{benzene}/D_{toluene}$ = 1.15 ± 0.06 (Hayduk and Laudie, 1974; Lide,

316 1994; Montgomery, 1996; Gabler et al., 1996; Rolle and Jin, 2017; Kopinke et al.,
317 2018). This criterion was fulfilled for all experiments presented in this study.
318 Long-term experiments over up to eight weeks of diffusion time with diluted aqueous
319 solutions of hydrophobic and volatile compounds such as benzene and toluene are
320 sensitive towards substrate losses. Despite careful precautions (see experimental
321 part), we have reason to suspect that such losses may have occurred when the upper
322 compartment of the diffusion cell was probed via gas samples from the headspace
323 above the stirred water phase. These losses could not be fully clarified. Therefore, we
324 consider these results with particular caution. The influence of losses on the isotope
325 pattern of diffusants can be minimized by extrapolation of the data towards short
326 diffusion times. The obtained data in Table 2 with headspace sampling (experiment
327 no. 4) are then in conformity with our general finding of nonsignificant diffusive isotope
328 fractionation of benzenes and toluenes.
329 The issue of long-term stability of our diaphragm cell was solved by application of an
330 organic extractant phase (n-octane) above the water phase in the destination
331 compartment, which acts as a steady sink of benzene and toluene, thus protecting
332 them from losses. This sink has the consequence that the real diffusant concentration
333 in the upper aqueous phase is kept close to zero through the entire diffusion time
334 ($C_{destin,i,initial} = C_{destin,i,t} \approx 0$).
335 Figure 4 shows typical concentration time profiles of benzene and toluene in two
336 separate diffusion experiments, one with *in-situ* extraction and another one with
337 headspace sampling. It is obvious that the slope is almost constant over time with *in-*
338 *situ* extraction of the upper compartment, whereas it levels off without this sink. From
339 the ratio of the initial slopes, the ratio $D_{benzene}/D_{toluene} = 1.15 \pm 0.05$ can be deduced.
340

→ Please insert **Figure 4** here: Kinetics of the diffusion of benzene and toluene in the diaphragm cell with 10 mL n-octane as extractant in the destination compartment (upper curves) and with 5 mL headspace gas phase (lower curves).

### *3.5. Isotope fractionation of benzene and toluene*

Table 2 summarizes results from four diffusion fractionation experiments with *in-situ* extraction and headspace sampling. The data are presented as ratios of isotopologue concentrations in the destination and the source compartments ($R$) at the end of the experiment. It is obvious from these data that there was no significant isotope fractionation, within an error range of about ± 5‰ for benzene and ± 10‰ for toluene. This finding is in contrast to the results of Jin et al. (2014) and of Rolle and Jin (2017), who found relatively large fractionation effects for the same target compounds (cf. data in Table 1). When the isotopic patterns in diffusate and retentate, expressed in terms of $R$, are not significantly different from 1.00, eq. 6 results in fractionation coefficients $\alpha_{diff}$ which are also not significantly different from 1.00. Applying the rules of error propagation to eq. 9, it follows that $\sigma(\alpha_{diff}) \approx \sigma(R)$, largely independent of the extent of diffusion $X$ and its uncertainty $\sigma(X)$.

**Table 2.** Ratios of concentrations of component pairs in the destination and the source compartment of the diaphragm cell after termination of four diffusion experiments. $R_{benzene}$ and $R_{toluene}$ are defined by $R = \left(\frac{C_{light}}{C_{heavy}}\right)_{destin} / \left(\frac{C_{light}}{C_{heavy}}\right)_{source}$ and $R_{benzene/toluene} = \left(\frac{C_{benzene}}{C_{toluene}}\right)_{destin} / \left(\frac{C_{benzene}}{C_{toluene}}\right)_{source}$

| Experiment no. | *t* in d | Extent of diffusion of $C_6H_6$ in % | $R_{benzene}$ | $R_{toluene}$ | $R_{benzene/toluene}$ |
|---|---|---|---|---|---|
| 1 | 57 | 34.5 | 0.997 ± 0.002[1)] | 0.999 ± 0.004 | 1.10 ± 0.03 |
| 2 | 17 | 11.9 | 0.995 ± 0.002 | 1.007 ± 0.008 | 1.13 ± 0.04 |
| 3 | 47 | 28.4 | 1.002 ± 0.003 | 1.007 ± 0.009 | 1.09 ± 0.05 |
| 4 [2)] | 11 | 7.2 | 1.003 ± 0.005 | 0.996 ± 0.010 | 1.14 ± 0.04 |

[1)] The error ranges indicate confidence intervals for P = 90% from 10 replicate analyses.

[2)] Experiment no. 4 was conducted with headspace sampling. Concentration ratios are extrapolated to *t* = 0.

Although the final isotope analysis of diffusate and retentate is sufficient for calculation of fractionation coefficients, in some diffusion experiments we also analysed the extraction phase in the upper compartment along the diffusion progress. Figure 5 illustrates such data (from experiment no. 1 in Table 2) for benzene and toluene along a diffusion time of 57 d. The isotopologue ratios in the diffusate are normalized to the initial composition in the source compartment of the diaphragm cell. The initial composition was simulated by an external reference sample. Please note that the two Y-axes in Figure 5 are staggered for better resolution of the two data sets. It is obvious from Figure 5 that (i) the isotope composition of the diffusate remains constant over the full range of the diffusion experiment (34.5% benzene transfer within 57 d) and (ii) the normalized isotopologue ratios are close to 1.00 for benzene and toluene.

→ Please insert **Figure 5** here: Isotope composition of benzene and toluene in the diffusate, normalized to the initial composition in the source compartment of the diaphragm cell over 57 days of diffusion time (data from experiment no. 1 in Table 1). Error bars indicate an estimate of two standard deviations of the mean value from 4 to 5 single analyses.

The benzene/toluene concentration ratios in Table 2 can be converted into ratios of diffusion coefficients by means of eq. 9. This results in $D_{benzene}/D_{toluene}$ = 1.11 ± 0.03 (1.080; 1.121; 1.075; 1.134 for the single experiments), which is within the range of literature values (1.15 ± 0.06, see above).

## 4. Conclusions

The present study investigates isotope fractionation between nondeuterated and perdeuterated benzenes and toluenes due to aqueous diffusion in a diaphragm cell. The results show no significant fractionation effects within a range of uncertainty of $|\varepsilon| \leq 5‰$ for benzene and ≤ 10‰ for toluene. These results are in conformity with previous data deduced from phase partitioning of deuterated compounds under kinetic control (Kopinke et al., 2018) and with the majority of diffusive fractionation data for isotopologues derived from other elements ($^{12}C/^{13}C$ and $^{35}Cl/^{37}Cl$) (Wanner and Hunkeler, 2019 and refs. cited there). However, our results are not consistent with the larger fractionation effects measured by Rolle and Jin (2017) and by Jin et al. (2014) for the same target compounds. The experimental techniques applied in all these studies are appropriate (cf. Table 2). At present, we cannot offer a plausible explanation for the obvious discrepancies.

It is notable that for aqueous-phase diffusive fractionation of argon isotopes there is a similar inconsistency of experimental data in the literature (cf. Table 1). The findings of

Tyroller et al. (2014) ($D_{40Ar}/D_{36Ar}$ = 0.948 ± 0.004) and more recently of Seltzer et al. (2019) ($k_{40Ar}/k_{36Ar}$ = 0.9963 ± 0.0003) are significantly different. Meanwhile, other groups have undertaken computational exercises in order to explain the unexpected strong diffusive fractionation of argon, which was not observed for neon, krypton and xenon isotopes (de Magalhaes et al., 2017). Such attempts can only be productive, however, when the underlying data base is solid.

If diffusive isotope effects are sensitive to solute-solvent interactions, the question may be allowed: how free is water in gels with 0.5 to 1 wt-% polysaccharides (agarose-like substances) as structure-forming agents and how “inert” are the structure builders? When we consider the inconsistent fractionation data for argon (see Table 1) it is noticeable that the *strong* fractionation was measured in a gel-stabilized water layer (Tyroller et al., 2014), whereas the *weak* fractionation was measured with free water bodies (Seltzer et al., 2019; Tempest and Emerson, 2013). The same discrepancy between fractionation data from gel-based measurements (Rolle and Jin, 2017; Jin et al., 2014; Rolle et al., 2010) and those from fluid water studies (Kopinke et al., 2018, and present study; LaBolle et al., 2008) applies for deuterated hydrocarbons (see Table 1). Based upon these findings, one could speculate about additional diffusant-matrix interactions in gel-based diffusion systems.

It was not the intent of this study to evaluate theoretical models for interpretation of diffusive isotope effects. Instead, we wish to contribute to a solid data base.

According to our diffusive fractionation data with perdeuterated compounds, it follows that for naturally occurring monodeuterated compounds only very small diffusion-related fractionation effects are to be expected in real aquifers. Thermodynamic fractionation effects due to adsorption and partitioning are much larger (Imfeld et al., 2014; Kopinke et al., 2017 and 2018).

**Acknowledgements**

The authors thank Mrs. Kerstin Lehmann for technical assistance in the experimental part. This research did not receive any specific grant from funding agencies in the public, commercial or not-for-profit sectors.

**Appendix A. Supplementary data**

Supplementary data to this article can be found online at …

## 5. References

Coplen, T.B., 2011. Guidelines and recommended terms for expression of stable-isotope-ratio and gas-ratio measurement results. Rapid Commun. Mass Spectrom. 25, 2538-2560.

Cussler, E.L., 2009. Diffusion: Mass Transfer in Fluid Systems. Cambridge University Press, Cambridge, 3rd ed.

Deacon, E.L., 1977. Gas transfer to and across an air/water interface. Tellus 29, 363-374.

de Magalhaes, H.P., Brennwald, M.S., Kipfer, R., 2017. Diverging effects of iostopic fractionation upon molecular diffusion of noble gases in water: mechanistic insights through *ab initio* molecular dynamics simulations. Environ. Sci. Proc. Impacts 19, 405-413.

Elsner, M., 2010. Stable isotope fractionation to investigate natural transformation mechanisms of organic contaminants: principles, prospects and limitations. J. Environ. Monitor. 12, 2005-2031.

Elsner, M., Jochmann, M.A., Hofstetter, T.B., Hunkeler, D., Bernstein, A., Schmidt, T.C., Schimmelmann, A., 2012. Current challenges in compound-specific stable

458 isotope analysis of environmental organic contaminants. Anal. Bioanal. Chem. 403,
459 2471–2491.
460 Gabler, T., Paschke, A., Schüürmann, G., 1996. Diffusion coefficients of substituted
461 benzenes at high dilution in water. J. Chem. Eng. Data 41, 33-36.
462 Hayduk, W., Laudie, H., 1974. Prediction of diffusion coefficients for non-electrolytes
463 in dilute aqueous solutions. AIChE J. 20, 611-615.
464 Hunkeler, D., Meckenstock, R.U., Sherwood Lollar, B., Schmidt, T.C., Wilson, J.T.,
465 2009**.** A guide for assessing biodegradation and source identification of organic
466 groundwater contaminants using compound specific isotope analysis (CSIA). U.S.
467 EPA, Washington, DC, Vol. EPA/600/R-08/148.
468 Imfeld, G., Kopinke, F.-D., Fischer, A., Richnow, H.-H., 2014. Carbon and hydrogen
469 fractionation of benzene and toluene during hydrophobic sorption in multistep batch
470 experiments. Chemosphere 107, 454-461.
471 Jähne, B., Heinz, G., Dietrich, W. 1987. Measurement of diffusion coefficients of
472 sparingly soluble gases in water. J. Geophys. Res*.* 92, 10767-10776.
473 Jin, B., Rolle, M., Li, T., Haderlein, S., 2014. Diffusive fractionation of BTEX and
474 chlorinated ethenes in aqueous solution: Quantification of spatial isotope gradients.
475 Environ. Sci. Technol. 48, 6141-6150.
476 Kopinke, F.-D., Georgi, A., Roland U., 2018. Isotope fractionation in phase-transfer
477 processes under thermodynamic and kinetic control – Implications for diffusive
478 fractionation in aqueous solution. Sci. Total Environ. 610-611, 495-502.
479 Kopinke, F.-D., Georgi, A., Imfeld, G., Richnow H.-H., 2017. Isotope fractionation of
480 benzene during partitioning – revisited. Chemosphere 168, 508-513.
481 Kopinke, F.-D., Georgi, A., Voskamp, M., Richnow, H.-H., 2005. Carbon isotope
482 fractionation of organic contaminants due to retardation on humic substances –

483 Implications for natural attenuation studies in aquifers. Environ. Sci. Technol. 39,
484 6052-6062.
485 LaBolle, E.M., Fogg, G.E., Eweis, J.B., Gravner, J., Leaist, D.G., 2008. Isotopic
486 fractionation by diffusion in groundwater. Water Resour. Res. 44 W07405.
487 Lide, D.R., 1994. CRC Handbook of chemistry and physics. 75th ed. CRC Press. p.
488 6.253.
489 Montgomery, J.H., 1996. Groundwater chemicals desk reference. 2nd ed., CRC Press,
490 U.S.
491 Rolle, M., Jin, B., 2017. Normal and inverse diffusive isotope fractionation of deuterated
492 toluene and benzene in aqueous systems. Environ. Sci. Technol. Letters 4, 298-
493 304.
494 Rolle, M., Chiogna, G., Bauer, R., Griebler, C., Grathwohl, P., 2010. Isotopic
495 fractionation by transverse dispersion: Flow-through microcosms and reactive
496 transport modeling study. Environ. Sci. Technol. 44, 6167-6173.
497 Schwarzenbach, R.P., Gschwend, P.M., Imboden, D.M., 2003. Environmental Organic
498 Chemistry. 2nd ed. Wiley-Interscience, pp. 808-811.
499 Seltzer, A.M., Ng, J., Severinghaus, J.P., 2019. Precise determination of Ar, Kr, and
500 Xe isotopic fractionation due to diffusion and dissolution in fresh water. Earth and
501 Planet Sci. Letters 514, 156-165.
502 Tempest, K.E., Emerson, S., 2013. Kinetic isotope fractionation of argon and neon
503 during air-water gas transfer. Marine Chem. 153, 39-47.
504 Thullner, M., Centler, F., Richnow, H.-H., Fischer, A., 2012. Quantification of organic
505 pollutant degradation in contaminated aquifers using compound specific stable
506 isotope analysis – Review of recent developments. Org. Geochem. 42, 1440-1460.

507 Tyroller, L., Brennwald, M.S., Busemann, H., Maden, C., Baur, H., Kipfer, R., 2018.
508 Negligible fractionation of Kr and Xe isotopes by molecular diffusion in water. Earth
509 and Planet Sci. Letters 492, 73-78.
510 Tyroller, L., Brennwald, M.S., Busemann, Mächler, L, Livingstone, D.M., Kipfer, R.,
511 2014. Fractionation of Ne and Ar isotopes by molecular diffusion in water. Geochim.
512 Cosmochim. Acta 136, 60-66.
513 Wanner, P., Hunkeler, D., 2019. Isotope fractionation due to aqueous phase diffusion
514 – What do diffusion models and experiments tell? – A review. Chemosphere 219,
515 1032-1043.
516 Wanner, P., Hunkeler, D., 2015. Carbon and chlorine isotopologue fractionation of
517 chlorinated hydrocarbons during diffusion in water and low permeability sediments.
518 Geochim. Cosmochim. Acta 157, 198-212.

519 List of figure captions:

520

521 **Figure 1.** Experimental set-up with diaphragm diffusion cell. Gaseous or liquid samples
522 can be taken through the Mininert™ valve.

523 **Figure 2.** Example of GC-MS isotope analyses of benzenes: ratios of peak areas for
524 ion traces m/z = 78 amu ($A_{78}$) and m/z = 84 amu ($A_{84}$) for samples (n-octane extracts)
525 of a typical diffusion experiment along the analysis numbers within a series of
526 successive analyses. The lines are guides for the eyes only.

527 **Figure 3.** Fractionation of isotopologues in a diffusion process with a sink in the
528 destination compartment according to the setup in Figure 1. Curves are calculated with
529 $D_{heavy}/D_{light}$ = 0.962 from Jin et al. (2014). The concentration ratios at the Y-axis are
530 normalized to the initial composition in the source compartment at $t$ = 0, except for the
531 dashed (red) curve, which represents the isotopologue ratios in the two compartments.

532 **Figure 4.** Kinetics of the diffusion of benzene and toluene in the diaphragm cell with
533 10 mL n-octane as extractant in the destination compartment (upper curves) and with
534 5 mL gas headspace phase (lower curve).

535 **Figure 5.** Isotope composition of benzene and toluene in the diffusate, normalized to
536 the initial composition in the source compartment of the diaphragm cell over 57 days
537 of diffusion time (data from experiment no. 1 in Table 2). Error bars indicate an estimate
538 of two standard deviations of the mean value from 4 to 5 single analyses.

539

**Figure 1.** Experimental set-up with diaphragm diffusion cell. Gaseous or liquid samples can be taken through the Mininert™ valve.

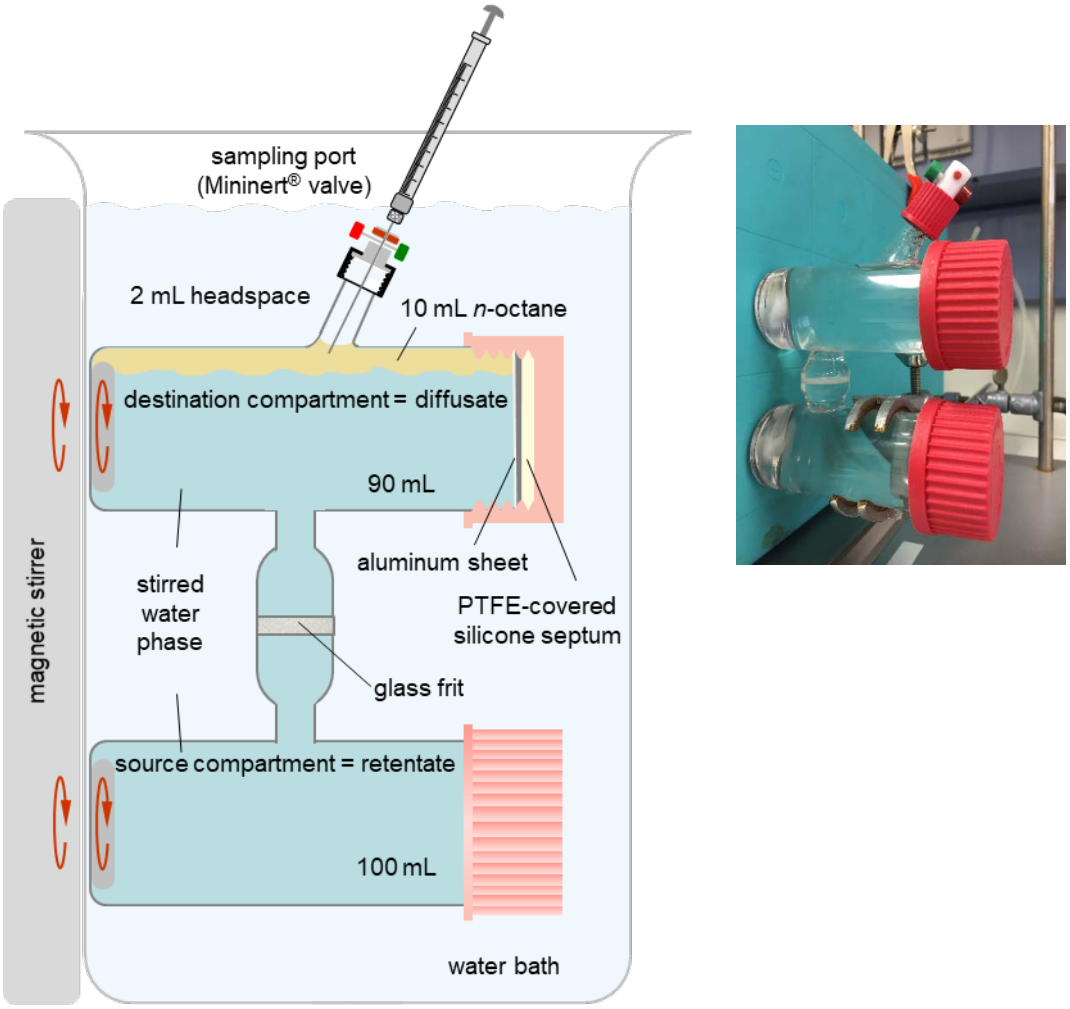

544 **Figure 2.** Example of GC-MS isotope analyses of benzenes: ratios of peak areas for
545 ion traces m/z = 78 amu ($A_{78}$) and m/z = 84 amu ($A_{84}$) for samples (n-octane extracts)
546 of a typical diffusion experiment along the analysis numbers within a series of
547 successive analyses. The lines are guides for the eyes only.

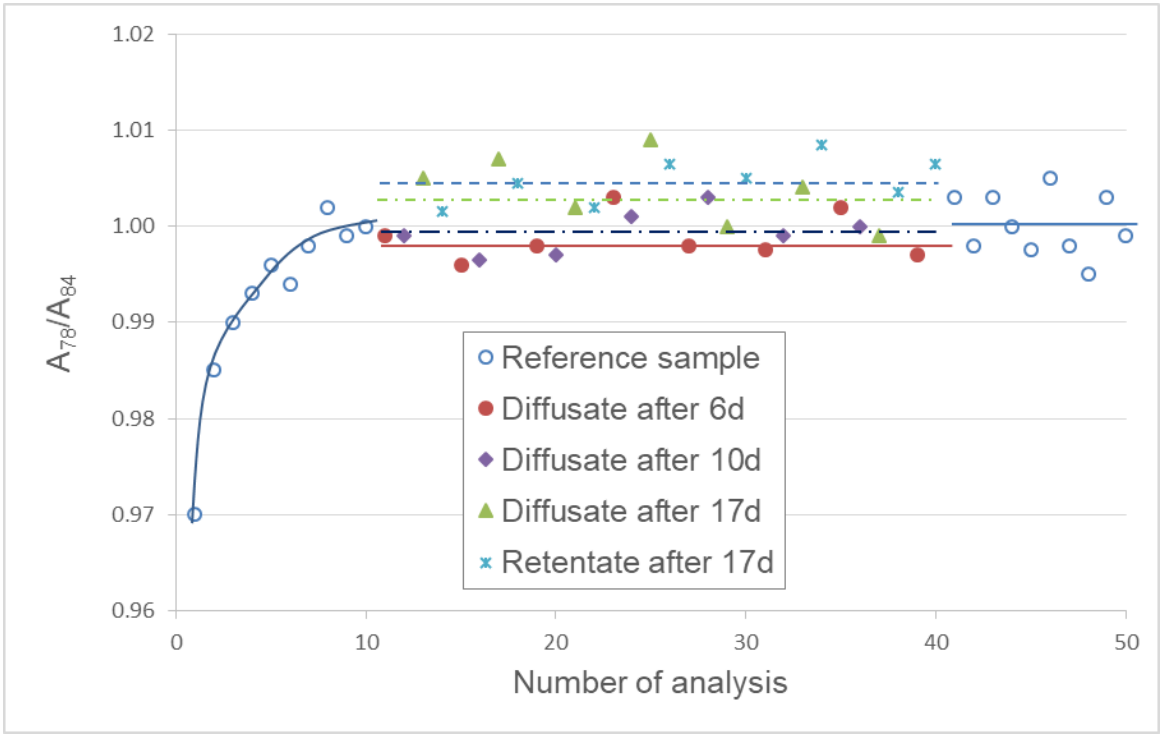


548

**Figure 3.** Predicted fractionation of isotopologues in a diffusion process with a sink in the destination compartment according to the setup in Figure 1. Curves are calculated with $D_{heavy}/D_{light}$ = 0.962 as reported in Jin et al. (2014). The concentration ratios at the Y-axis are normalized to the initial composition in the source compartment at $t$ = 0, except for the dashed (red) curve, which represents the isotopologue ratios in the two compartments.

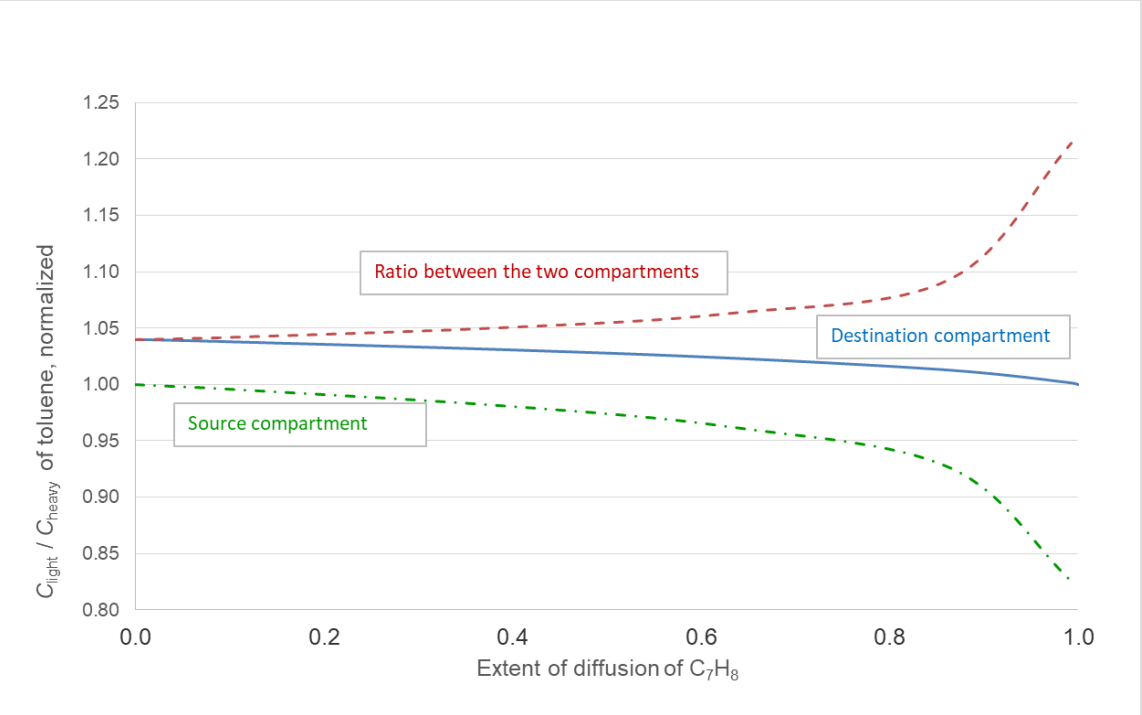


549

**Figure 4.** Kinetics of the diffusion of benzene and toluene in the diaphragm cell with 10 mL n-octane as extractant (*in-situ* extraction) in the destination compartment (upper curves) and with 5 mL gas headspace phase (lower curves).

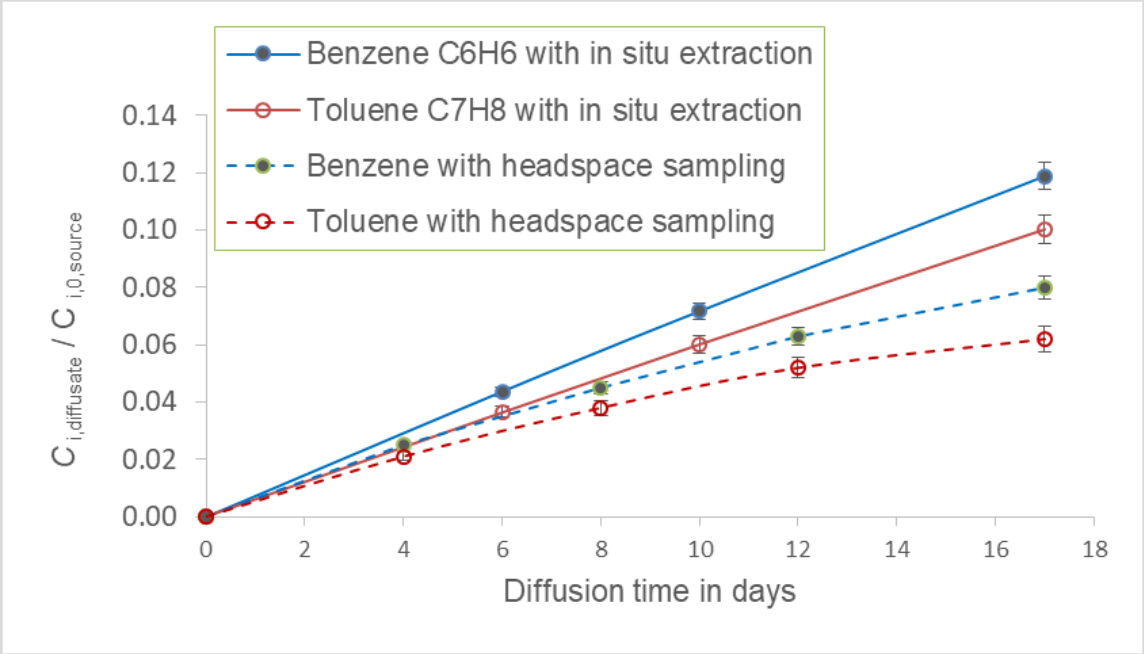


**Figure 5.** Isotope composition of benzene and toluene in the diffusate, normalized to the initial composition in the source compartment of the diaphragm cell over 57 days of diffusion time (data from experiment no. 1 in Table 2). Error bars indicate an estimate of two standard deviations of the mean value from 4 to 5 single analyses.